Journal of Materials Chemistry C

RSC Publishing

PAPER

View Article Online
View Journal | View Issue

Published on 21 December 2012. Downloaded by Ajou University Central Library on 2/3/2026 3:13:39 AM.

Cite this: *J. Mater. Chem. C*, 2013, **1**, 1595

Bandgap engineering of graphene by corrugation on lattice-mismatched MgO (111)

Sung Beom Cho and Yong-Chae Chung*

Received 24th September 2012
Accepted 20th December 2012

DOI: 10.1039/c2tc00257d

www.rsc.org/MaterialsC

The corrugation pattern and electronic structure of graphene on MgO (111), which is a lattice-mismatched substrate, were investigated using the *ab initio* method. On Mg-terminated octo-polar reconstructed MgO (111), graphene was physisorbed and shaped into a stripe-like corrugation pattern. Due to weak charge transfer at the interface, the graphene was of the n-type doped, and its low effective mass was preserved. On the other hand, graphene on O-terminated octo-polar reconstructed MgO (111) showed a larger corrugation triggered by periodic oxygen–carbon chemisorption. In addition, a band-gap opening, which was induced by the periodic chemisorption, of 0.294 eV was observed. The results indicate that a corrugation structure induced by the lattice-mismatched substrate is highly effective for band-gap engineering treatment.

1 Introduction

Graphene is one of the most promising materials for future applications in nanoelectronic devices due to its unique electrical, physical, and optical properties.[1,2] However, despite its extraordinary properties, one of the biggest hurdles in realizing graphene-based electronics is its zero-gap nature. Due to the absence of a bandgap, graphene-based devices cannot be switched off, which is a serious obstacle in designing digital logic circuits. Thus, the bandgap engineering[3] of graphene applications in electronics is critical. An effective way to induce a bandgap is by fabricating graphene by employing a superstructure such as a nanoribbon,[4,5] quantum dot,[6,7] or nanomesh.[8] These superstructures induce a quantum confinement effect that opens the bandgap, but unresolved issues remain related to the fabrication. Top-down approaches such as lithography or etching cannot guarantee uniform width, or a well-defined edge of superstructures under 10 nm. Recently, however, production of a reliable structure was achieved using a bottom-up approach.[9] However, extension to the semiconductor substrate and the transfer process of the patterned nanoribbons still remain hurdles. One of the most promising alternatives is to decorate graphene by using suitable adsorbates.[10–13] However, when the geometry of the adsorbates is not well-ordered, the adsorbates can induce interband trapping or additional scattering resulting in serious degradation of the performance of the device. Another way to open the bandgap is by placing graphene onto a specific substrate such as SiC,[14] Al_2O_3,[15] or BN.[16] These substrates form an epitaxial interface with graphene that induces the breaking of the AB sublattice symmetry of the graphene. This substrate-induced method has an obvious technical advantage due to its simple process.

However, graphene can be placed not only on the epitaxial substrate but also on the lattice-mismatched substrate with corrugation. When a lattice-mismatch is introduced to graphene, it cannot be sufficiently stretched for the lattice of the substrate due to the strength of the C–C bonds. Instead, the moiré structures between the graphene and the substrate have only incommensurate or weakly commensurate superperiodicity.[17] The structures are connected with a buckling of the graphene layer, indicating local variations of the graphene–substrate adhesion. The corrugation structure of graphene depends on the strength and local variation of the adhesion between the graphene and the substrate, which ranges from strong chemisorption to weak physisorption.[18] Moreover, it has been confirmed that corrugation of graphene is partially regulated by the surface morphology of various substrates (*e.g.* GaAs, InGaAs or SiO_2).[19,20] Depending on the graphene–substrate interfacial bonding energy and the substrate surface morphology, the corrugation structure of graphene ranges from closely conforming to the substrate to remaining flat on the substrate. Therefore, the substrate-regulated corrugation of graphene induced by the lattice-mismatched substrate can be a fascinating tuning method for the electronic structure of graphene.

In this study, band gap engineering was performed with quasi-periodicity induced by a lattice-mismatched substrate. The chosen substrate was MgO (111) which has been demonstrated to have advantages in implementation of Si-based technology[21] and deposition of a single layer of graphene.[22] The corrugation structure of graphene on MgO (111) and its related electronic structure were analyzed using first-principles calculation.

Computational Materials Science and Engineering Laboratory, Department of Materials Science and Engineering, Hanyang University, Seoul, Korea. E-mail: yongchae@hanyang.ac.kr

Published on 21 December 2012. Downloaded by Ajou University Central Library on 2/3/2026 3:13:39 AM.

2 Calculation details

First-principles calculations based on density functional theory were performed with the Vienna *ab-initio* simulation package (VASP).[23] The projector augmented wave (PAW) method[24] was used to describe the interactions of the valence electrons with their atomic cores, and the exchange-correlation function between the electrons was adopted for the Perdew, Burke, and Ernzerhof (PBE) potential.[25] In all our PAW calculations, the C and O atoms were described with a $1s^2$ core. For the Mg atom, we used a $1s^2 2s^2 2p^6$ core (large core). Throughout, a plane-wave basis set was employed to describe a valence electron with a kinetic energy cutoff of 450 eV. The electronic structure was calculated using the Gaussian-smearing method with a width of 0.02 eV. The effect of the van der Waals interaction was modeled by employing the semi-empirical correction scheme of Grimme (DFT+D2),[26] which has been proven to be successful in describing the geometries of graphene-related structures.[15,27] The supercell of graphene on the MgO (111) polar surface was modeled by symmetric slabs that can cancel out internal dipole moments of the polar surface. The simulated slab models consist of 2 layers of (5×5) graphene on 13 layers of the MgO (111) substrate with the corresponding periodicity. The vacuum distance should be carefully controlled to avoid the interference between the supercells. In this study, a minimum vacuum distance of 10 Å was carefully chosen considering computational convenience and previous MgO (111) polar surface study.[28] The three central atomic layers of the substrates were kept fixed in the structure optimization process while the outer atomic layers were relaxed until the maximum total Hellmann–Feynman forces were in the range of 0.05 eV $Å^{-1}$. The *k*-point integration was made with a $3 \times 3 \times 1$ Monkhorst–Pack grid[29] for fast ionic relaxation and a $7 \times 7 \times 1$ grid to obtain an accurate electronic structure.

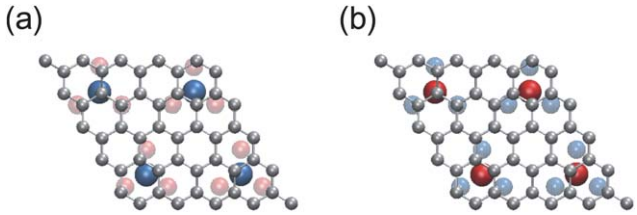

Fig. 1 Top view of the graphene on an Mg-terminated octopolar MgO (111) surface and an O-terminated octopolar MgO (111) surface. Due to the surface reconstruction, the periodicity of MgO and graphene is 2 : 5. The transparent atoms represent the subsurface atoms of MgO (111). Gray, red, and blue atoms represent the C, O, and Mg atoms.

3 Results and discussion

Graphene was then deposited onto a bulk-like MgO (111) surface, but a reconstructed MgO (111) surface. Along the (111) direction, the stacking of the rocksalt MgO consists of alternating layers of positively charged Mg ion and negatively charged O ion. This alternative structure generates an infinite electrostatic dipole field perpendicular to the surface which diverges the surface energy of the bulk-terminated polar surface.[30] To cancel out the electrostatic dipole, surface reconstruction occurs on the polar surface.[31] In the case of MgO, the most stable reconstructed surface configuration is known as the Mg-terminated (Mg-octo) and O-terminated (O-octo) $p(2 \times 2)$ octopolar reconstruction according to the DFT surface phase diagram calculation by Zhang and Tang.[28] The surface phase diagram indicated that the Mg and O terminated octopolar reconstructed surface had an almost degenerate surface energy. The octopolar reconstruction consists of a pyramidal structure in which 3/4 of the ions in the outer most layers and 1/4 of the ions in the second layer are missing. The periodicity of the

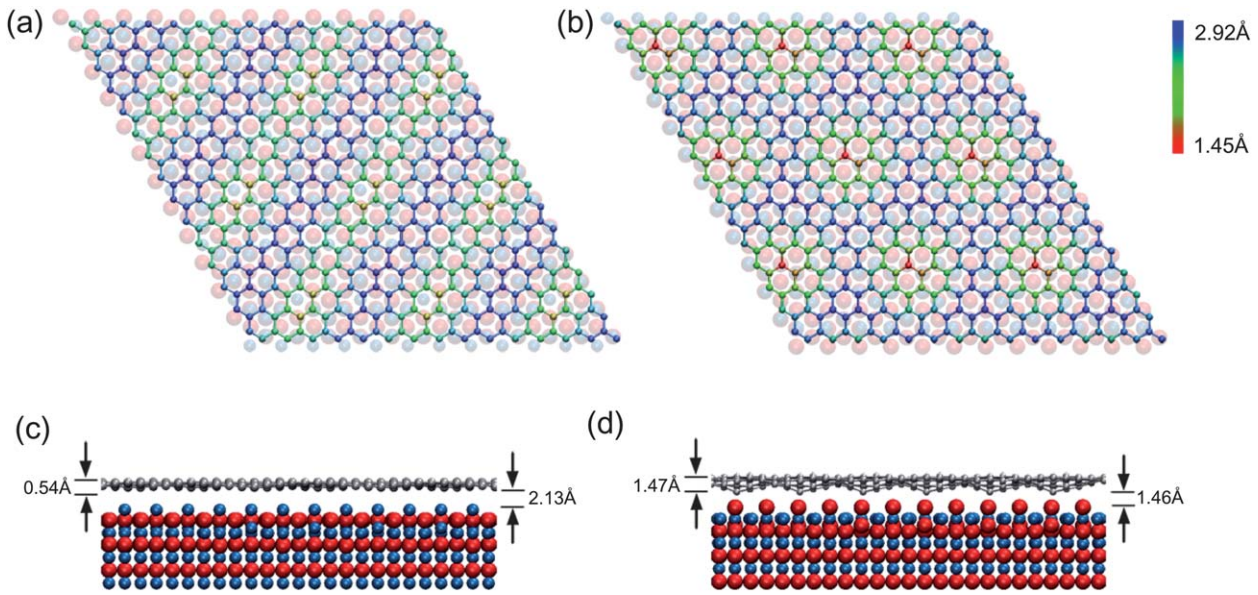

Fig. 2 The corrugation structure of graphene/MgO (111). (a) and (b) are the top view of graphene on Mg-octo and O-octo, respectively. The stripe-like corrugated pattern is formed in the graphene on Mg-octo, while the dip region is periodically formed in the graphene on O-octo. The formed dip region results from the C atom moving down from the apex of the pyramid. (c) and (d) are the side view of graphene on Mg-octo and O-octo. The graphene corrugation is relatively flat on the Mg-octo while the corrugation is large on the O-octo.

 This journal is © The Royal Society of Chemistry 2013

Published on 21 December 2012. Downloaded by Ajou University Central Library on 2/3/2026 3:13:39 AM.

2 pyramids of MgO (111) (6 Å × 2 = 12 Å) corresponded to a 5 graphene unit cell (2.45 Å × 5 = 12.25 Å). The coincidence unit cell of graphene on the O-octo and Mg-octo substrate is shown in Fig. 1. The lattice mismatch between graphene and MgO (111) prevents every carbon atom from occupying the apex site of the pyramid. Instead, only one of the four pyramids in the coincidence unit cell is precisely occupied by one of the fifty carbon atoms. Because of the pyramidal structure of the reconstructed MgO surface, the structure of the graphene depends on the termination of the MgO surface.

The resulting structure shapes the regulation pattern of the corrugated graphene. Fig. 2a and c show the stripe-like corrugation structure of graphene on Mg-octo and the striped moiré pattern was arrayed along the [1$\bar{1}$0] direction which was the dense-packed direction of graphene and MgO. The hump region of the stripe included C atoms atop the pyramid, while the dip region was the interval region of the pyramid. The height of the hump region was 2.67 Å while that of the dip region was 2.13 Å. This corrugation (0.54 Å) and stripe pattern along the densed-packed direction are comparable to graphene on Ir (111).[32,33] On the other hand, the graphene on O-octo does not show a striped-corrugation pattern as shown in Fig. 2b and d. Instead, the C atom on the apex of the pyramid moved down to 1.47 Å and generated a dip region around itself. The distance between the C atom and the O atom of the pyramid was 1.46 Å which was in the range of typical chemisorption of the graphene–substrate.[34,35] The corrugation pattern of graphene on O-octo is regulated by the strong interaction between the pyramid and the C atom on the apex site. A large corrugation of the graphene of 1.47 Å on O-octo is comparable to graphene/Ru (0001) and graphene/Rh (111).[36]

To understand the relationship between the corrugation pattern and the substrate termination, the adhesion character was investigated. The performed DFT-D2 calculation was based on the polarizability of neutral atoms. Hence, the calculated dispersion energy in this study, which is the case between the ion (Mg or O) and C atom, may not be quantitatively accurate one.[37,38] Although more accurate adhesion energy may be obtained in computationally more computationally expensive calculation scheme, it is believed that the essential features of the adhesion are correctly described. For the graphene on Mg-octo, the adhesion energy calculated in GGA was 1.5 eV for 50 C atoms (+30 meV per C atom), while the adhesion energy implementing DFT-D2 was −2.7 eV for 50 C atoms (−54 meV per C atom). This result indicates that the contribution of the adhesion is mainly due to the van der Waals force. This impression becomes clear when analyzing the charge redistribution and density of states. Fig. 3a shows the electron density difference between the interface and the sum of the separate graphene and MgO (111) surface. The electron redistribution

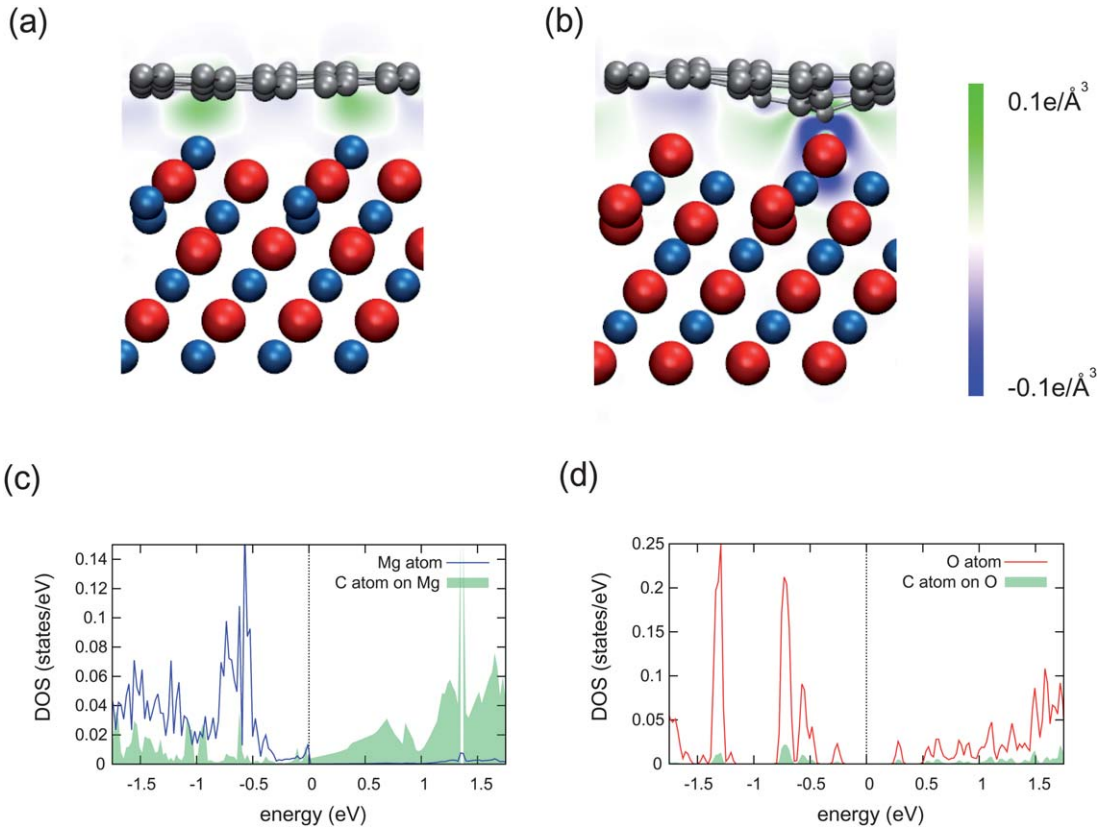

Fig. 3 The electron density difference between the (a) graphene/Mg-Octo and (b) graphene/O-octo. The redistributed electron is small and localized at the interfacial region in graphene/Mg-octo. On the other hand, a large charge transfer occurs including the atomic region in graphene/O-octo. (c) and (d) are the density of states of the apex atom of the pyramid and the C atom on the apex site in the graphene/Mg-octo and graphene/O-octo system. The C atom does not show significant hybridization with a pyramid in graphene/Mg-octo. In contrast, the C atom is strongly hybridized with the O atom of the pyramid in graphene/O-octo.

Published on 21 December 2012. Downloaded by Ajou University Central Library on 2/3/2026 3:13:39 AM.

did not include the atomic regions but only the weakly localized interfacial region. In addition, the density of state analysis indicates that there were no remarkable hybridized states between the C atom and the Mg atom of the pyramid, as shown in Fig. 3c. The adhesion character of graphene on Mg-octo is mainly physisorption due to the van der Waals interaction. For the graphene on O-octo, the adhesion energy of the 50 C atoms is −1.8 eV, but the main adhesion mechanism is not only physisorption, but also the van der Waals interaction; it is believed that the C atom on the apex of the pyramid, which moved down to the apex and induced a large corrugation, can be the dominant factor in adhesion. To understand the adhesion character, the electron redistribution and density of states analysis were conducted using the same techniques as graphene/Mg-octo. The electron redistribution analysis of Fig. 3b shows a remarkable charge transfer between the pyramid and the C atom on the apex site. The redistributed electrons were much larger than the graphene/Mg-octo and also included the atomic region. The electron was depleted in the interfacial and pyramidal region, but accumulated in the atomic region of carbon. The density of state analysis in Fig. 3d indicates that the redistributed electron between the C atom and the O atom in the pyramid formed a covalent bond. While the pristine graphene showed a metallic property due to π bonding, the carbon atom on the pyramid showed strong orbital hybridization with an oxygen atom. This result indicates that the C atom on the apex site has sp^3 bond character forming the chemical bond with the apex O atom of the pyramid. The graphene on the O-octo has periodic chemisorption between the C atom on the apex site and the apex O atom of the pyramid and this chemisorption dominantly contributes to the adhesion.

The corrugation pattern can be inferred by the adhesion character between the graphene and the lattice-mismatched substrate. Where the adhesion mechanism shows mainly physisorption such as graphene/Mg-octo, the energy difference between the favorable adsorption site and the unfavorable site is relatively small. When a lattice mismatch is introduced into the physisorbed graphene, graphene becomes corrugated to reduce the strain energy rather than to keep a favorable adsorption site. The graphene will buckle in the loose-packed direction because this direction minimizes the stretch of the C–C bond. Therefore, a stripe pattern is observed along the most densely packed direction in the corrugation. In contrast, in the case of chemisorption such as graphene/O-octo, the energy difference between the adsorption site is considerable, leading to regulation of the graphene layer. The chemical bond between the graphene and the substrate strongly anchors the bonded C atoms and only the other carbons except the pinned

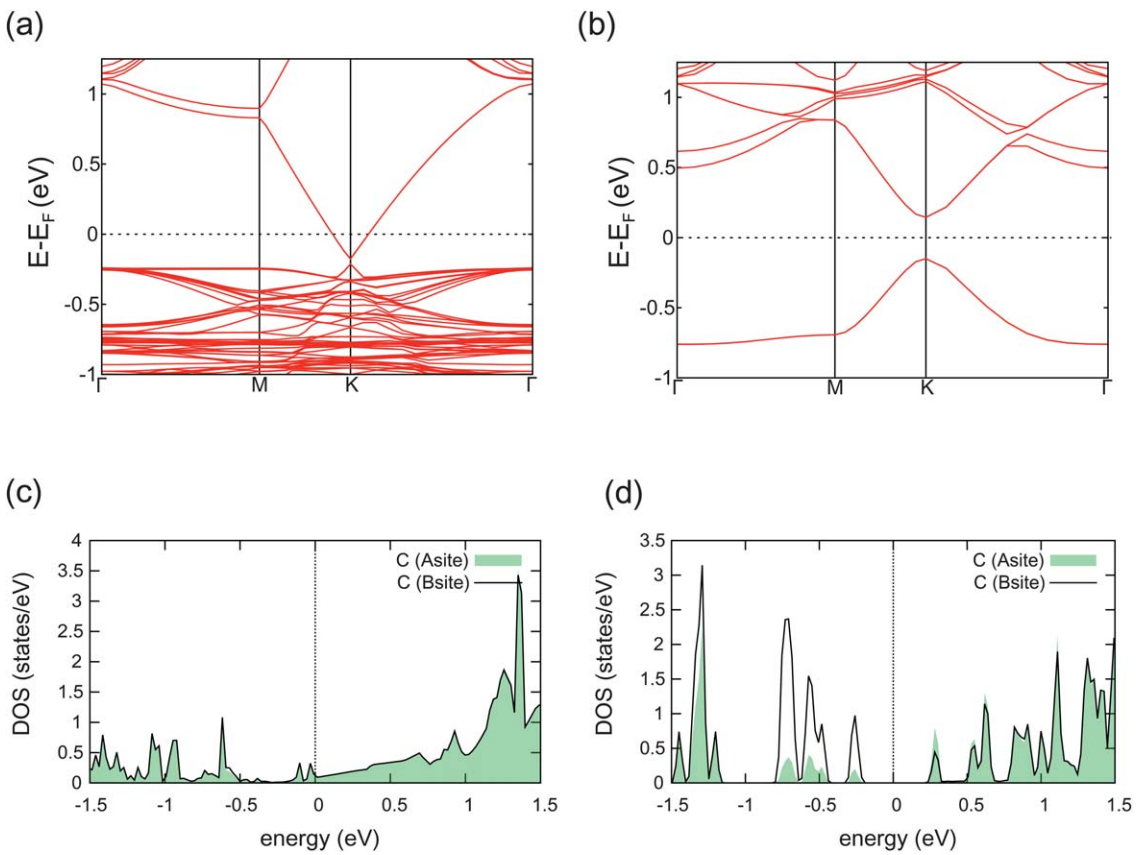

Fig. 4 The band structure of (a) graphene/Mg-octo and (b) graphene/O-octo. The graphene on the Mg-octo is n-type doped preserving the high mobility of the conduction band. A band gap of 0.294 eV is observed in graphene on O-octo. (c) and (d) are the local density of states of the AB sublattice of graphene on Mg-Octo and O-octo. The A site includes the C atom on the apex of the pyramid, while the B site does not include it. The density of states of the AB sublattice are identical in the graphene/Mg-octo. In contrast, the density of states are not identical in the graphene/O-octo.

 This journal is © The Royal Society of Chemistry 2013

Published on 21 December 2012. Downloaded by Ajou University Central Library on 2/3/2026 3:13:39 AM.

C become largely corrugated. The corrugation pattern depends significantly on the adhesive character between the graphene and the substrates.

The adsorption features also induce significant changes in the electronic structure of the graphene. Fig. 4a shows the band structure of graphene on Mg-octo which is n-type doped. The lowest conduction band of the graphene is partially occupied, while the valence band below the Fermi level coexists with a band of MgO. This n-type doping can be explained by the additional electron from the electron redistribution, as shown in Fig. 3a. According to our Bader charge analysis, the transferred charge from the MgO surface to the graphene is 0.008 eV per C atom. Also, the band of graphene near the Fermi level is still linear, which indicates that its low effective mass is preserved. On the other hand, in the case of graphene on O-octo, a remarkable band gap opening of 0.294 eV was observed as shown in Fig. 4b. Because the calculated bandgap in the conventional DFT is underestimated[39,40] by 30–100%, the actual band gap is expected to be larger than 0.4 eV, which is the required gap for a sufficient on/off ratio in graphene-based field effect transistors.[41] The bandgap opening of graphene on O-octo can be inferred by the sublattice symmetry breaking induced by the periodic chemisorption. The primitive unit cell consists of two carbon atoms that occupy the A and B sublattices, respectively. Where the graphene is placed on the MgO (111) substrate, only one of the AB sublattices can occupy the apex site of the pyramid. The local density of states analysis of each of the two sublattices presented in Fig. 4c and d shows the sublattice symmetry of graphene on the MgO (111) substrate.

The electronic structure of each sublattice of graphene on Mg-octo is almost identical due to the weak interaction between the pyramid and the C atom. In contrast, the strong interaction between the pyramid of the O-octo and C atoms changes the electronic structure of the sublattice, leading to a break in the sublattice symmetry. As shown in Fig. 3d and 4b, the carbon on the pyramid of the O-octo forms sp^3 hybridization, and this hybridization induces a split of the π–π^* state degeneracy. Moreover, the new energy states are formed by hybridization between the π states and the 2p orbital of O. This significant change in the electronic structure is not localized around the chemisorption region but uniformly delocalized. It can be inferred that the chemisorption is repeated through the entire graphene and the periodicity is enough to affect the entire electronic structure.

4 Conclusions

The corrugation structure and the induced electronic structure on the lattice-mismatched oxide substrate, an Mg-terminated and an O-terminated octopolar reconstructed MgO (111) surface, was investigated. The corrugation was found to regulate the graphene structure and generate a periodic interaction with the substrate. On the Mg-terminated octopolar reconstructed MgO (111) substrate, graphene remained conductive while preserving its high mobility. In contrast, a band gap of 0.294 eV appeared in the graphene layer on the O-terminated octopolar reconstructed MgO (111) substrate. From this remarkable bandgap opening, it can be inferred that the periodic chemisorption of the corrugated graphene can break the sublattice symmetry. This new bandgap engineering method using a lattice-mismatched substrate is an important step toward the realization of graphene-based electronics.

Acknowledgements

This work was supported by a National Research Foundation (NRF) grant funded by the Korean Ministry of Education, Science and Technology (MEST) grant (no. 2010-0023761), the project of Global PhD Fellowship (no. 2011-0007330) conducted by the NRF in 2011, and the Basic Science Research Program through the NRF of Korea funded by the MEST (no. 2011-0016945).

References

1 K. S. Novoselov, A. K. Geim, S. V. Morozov, D. Jiang, Y. Zhang, S. V. Dubonos, I. V. Grigorieva and A. A. Firsov, *Science*, 2004, **306**, 666–669.
2 K. Novoselov, A. Geim, S. Morozov, D. Jiang, M. Grigorieva, S. Dubonos and A. Firsov, *Nature*, 2005, **438**, 197–200.
3 K. Novoselov, *Nat. Mater.*, 2007, **6**, 720–721.
4 M. Han, B. Özyilmaz, Y. Zhang and P. Kim, *Phys. Rev. Lett.*, 2007, **98**, 206805.
5 X. Li, X. Wang, L. Zhang, S. Lee and H. Dai, *Science*, 2008, **319**, 1229–1232.
6 L. Ponomarenko, F. Schedin, M. Katsnelson, R. Yang, E. Hill, K. Novoselov and A. Geim, *Science*, 2008, **320**, 356–358.
7 B. Trauzettel, D. Bulaev, D. Loss and G. Burkard, *Nat. Phys.*, 2007, **3**, 192–196.
8 J. Bai, X. Zhong, S. Jiang, Y. Huang and X. Duan, *Nat. Nanotechnol.*, 2010, **5**, 190–194.
9 J. Cai, P. Ruffieux, R. Jaafar, M. Bieri, T. Braun, S. Blankenburg, M. Muoth, A. Seitsonen, M. Saleh, X. Feng, *et al.*, *Nature*, 2010, **466**, 470–473.
10 R. Balog, B. Jørgensen, L. Nilsson, M. Andersen, E. Rienks, M. Bianchi, M. Fanetti, E. Lægsgaard, A. Baraldi, S. Lizzit, *et al.*, *Nat. Mater.*, 2010, **9**, 315–319.
11 F. Yavari, C. Kritzinger, C. Gaire, L. Song, H. Gulapalli, T. Borca-Tasciuc, P. Ajayan and N. Koratkar, *Small*, 2010, **6**, 2535–2538.
12 S. Kozlov, F. Viñes and A. Görling, *Adv. Mater.*, 2011, **23**, 2638–2643.
13 H. Liu, Y. Liu and D. Zhu, *J. Mater. Chem.*, 2010, **21**, 3335–3345.
14 S. Zhou, G. Gweon, A. Fedorov, P. First, W. De Heer, D. Lee, F. Guinea, A. Neto and A. Lanzara, *Nat. Mater.*, 2007, **6**, 770–775.
15 B. Huang, Q. Xu and S. Wei, *Phys. Rev. B: Condens. Matter*, 2011, **84**, 155406.
16 G. Giovannetti, P. Khomyakov, G. Brocks, P. Kelly and J. Van Den Brink, *Phys. Rev. B: Condens. Matter*, 2007, **76**, 073103.
17 J. Wintterlin and M. Bocquet, *Surf. Sci.*, 2009, **603**, 1841–1852.

Published on 21 December 2012. Downloaded by Ajou University Central Library on 2/3/2026 3:13:39 AM.

18 A. Preobrajenski, M. Ng, A. Vinogradov and N. Mårtensson, *Phys. Rev. B: Condens. Matter*, 2008, **78**, 073401.
19 V. Geringer, M. Liebmann, T. Echtermeyer, S. Runte, M. Schmidt, R. Rückamp, M. Lemme and M. Morgenstern, *Phys. Rev. Lett.*, 2009, **102**, 76102.
20 U. Stöberl, U. Wurstbauer, W. Wegscheider, D. Weiss and J. Eroms, *Appl. Phys. Lett.*, 2008, **93**, 051906.
21 H. Yu and J. Lee, *Cryst. Growth Des.*, 2010, **10**, 5200–5204.
22 S. Gaddam, C. Bjelkevig, S. Ge, K. Fukutani, P. Dowben and J. Kelber, *J. Phys.: Condens. Matter*, 2011, **23**, 072204.
23 G. Kresse and J. Furthmüller, *Phys. Rev. B: Condens. Matter*, 1996, **54**, 11169.
24 P. Blöchl, *Phys. Rev. B: Condens. Matter*, 1994, **50**, 17953.
25 J. Perdew, K. Burke and M. Ernzerhof, *Phys. Rev. Lett.*, 1996, **77**, 3865–3868.
26 S. Grimme, *J. Comput. Chem.*, 2006, **27**, 1787–1799.
27 T. Bucko, J. Hafner, S. Lebegue and J. Angyán, *J. Phys. Chem. A*, 2010, **114**, 11814–11824.
28 W. Zhang and B. Tang, *J. Phys. Chem. C*, 2008, **112**, 3327–3333.
29 H. Monkhorst and J. Pack, *Phys. Rev. B: Solid State*, 1976, **13**, 5188–5192.
30 P. W. Tasker, *J. Phys. C: Solid State Phys.*, 1979, **12**, 4977.
31 D. Wolf, *Phys. Rev. Lett.*, 1992, **68**, 3315–3318.
32 A. NDiaye, S. Bleikamp, P. Feibelman and T. Michely, *Phys. Rev. Lett.*, 2006, **97**, 215501.
33 C. Busse, P. Lazić, R. Djemour, J. Coraux, T. Gerber, N. Atodiresei, V. Caciuc, R. Brako, A. NDiaye, S. Blügel, *et al.*, *Phys. Rev. Lett.*, 2011, **107**, 36101.
34 S. Kozlov, F. Viñes and A. Görling, *J. Phys. Chem. C*, 2012, **116**, 7360–7366.
35 M. Iannuzzi and J. Hutter, *Surf. Sci.*, 2011, **605**, 1360–1368.
36 B. Wang, M. Bocquet, S. Marchini, S. Günther and J. Wintterlin, *Phys. Chem. Chem. Phys.*, 2008, **10**, 3530–3534.
37 G. Zhang, A. Tkatchenko, J. Paier, H. Appel and M. Scheffler, *Phys. Rev. Lett.*, 2011, **107**, 245501.
38 W. Reckien, F. Janetzko, M. Peintinger and T. Bredow, *J. Comput. Chem.*, 2012, **33**, 2023.
39 C. S. Wang and W. E. Pickett, *Phys. Rev. Lett.*, 1983, **51**, 597–600.
40 M. K. Y. Chan and G. Ceder, *Phys. Rev. Lett.*, 2010, **105**, 196403.
41 F. Schwierz, *Nat. Nanotechnol.*, 2010, **5**, 487–496.

 This journal is © The Royal Society of Chemistry 2013